JACS
JOURNAL OF THE AMERICAN CHEMICAL SOCIETY
Article
pubs.acs.org/JACS

Electrocatalytic Activity of Individual Pt Nanoparticles Studied by Nanoscale Scanning Electrochemical Microscopy

Jiyeon Kim,[†] Christophe Renault,[‡] Nikoloz Nioradze,[†] Netzahualcóyotl Arroyo-Currás,[§] Kevin C. Leonard,[∥] and Allen J. Bard*[,†]

[†]Center for Electrochemistry, Department of Chemistry, The University of Texas at Austin, Austin, Texas 78712, United States
[‡]Laboraoire de Physique de la Matière Condensée, Ecole Polytechnique, 91128 Palaiseau, France
[§]Department of Chemistry and Biochemistry, University of California Santa Barbara, Santa Barbara, California 93111, United States
[∥]Center for Environmentally Beneficial Catalysis, Department of Chemical and Petroleum Engineering, The University of Kansas, Lawrence, Kansas 66047, United States

Supporting Information

ABSTRACT: Understanding the relationship between the structure and the reactivity of catalytic metal nanoparticles (NPs) is important to achieve higher efficiencies in electrocatalytic devices. A big challenge remains, however, in studying these relations at the individual NP level. To address this challenge, we developed an approach using nanometer-scale scanning electrochemical microscopy (SECM) for the study of the geometric property and catalytic activity of individual Pt NPs in the hydrogen oxidation reaction (HOR). Herein, Pt NPs with a few tens to a hundred nm radius were directly electrodeposited on a highly oriented pyrolitic graphite (HOPG) surface via nucleation and growth without the necessity of capping agents or anchoring molecules. A well-defined nanometer-sized tip comparable to the dimensions of the NPs and a stable nanogap between the tip and NPs enabled us to achieve lateral and vertical spatial resolutions at a nanometer-scale and study fast electron-transfer kinetics. Specifically, the use of two different types of redox mediators: (1) outer-sphere mediator and (2) inner-sphere mediators could differentiate between the topography and the catalytic activity of individual Pt NPs and measure a large effective rate constant of HOR, k^0_{eff} of ≥2 cm/s as a lower limit at each Pt NP. Consequently, the size, shape, spatial orientation and the catalytic activity of Pt NPs could be determined at an individual level in nanoscale SECM where imaging accompanied by theoretical modeling and analysis. This approach can be easily extended to quantitatively probe the effects of the surface property, such as capping agent effects on the catalytic activity of a variety of metal NPs for the design and assessment of NP catalysts.

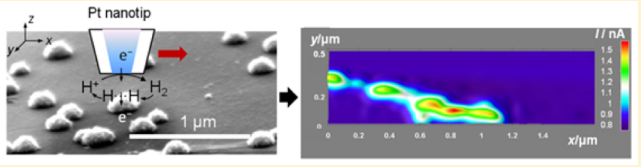

1. INTRODUCTION

Scanning electrochemical microscopy (SECM) is an imaging technique capable of providing chemical and topographic information, especially about surfaces immersed in a solution. It is based on moving a small tip electrode very close to a substrate surface. Unlike optical methods, it is unfettered by diffraction limits, and it does not require high energy or intensity irradiation. Most of the SECM studies have been carried out with the resolution of the order of micrometers, but pioneering studies by Amemiya, Mirkin, and our group have suggested that nm resolution is possible.[1,2]

However, imaging at the nm level is challenging, and a number of new factors must be considered. The tip size and its distance from the surface largely govern the resolution. Plus nm-size tips are fragile and subject to destruction by electrostatic effects and vibrations. They are also easily contaminated, so extremely pure solutions are needed. Positioning and maintaining the tip at nm distances requires high positional stability. Unlike scanning tunneling and atomic force microscopy, in the SECM the tip does not ever contact the surface. This requires a high level of control of the positioners and the system temperature.

Metal nanoparticles (NPs) are excellent catalysts with a uniquely high surface-to-volume ratio[3] that can be deposited and supported on solid electrodes for important real-life applications such as energy production, e.g., fuel cells.[4] Because of the widespread scientific and industrial interest in the catalytic properties of NPs, numerous investigations have been carried out seeking to deliberately control the size, shape, and surface properties of NPs to achieve higher efficiencies in their catalytic activities, with particular focus on improving the efficiency of electrochemical energy conversion and storage processes.[5,6] Such an effort, however requires a fundamental understanding of how these properties are correlated with the catalytic activity at each individual NP level not an ensemble. Therefore, the ability to determine or probe electrochemical activity at nanometer-scale becomes important.

Received: April 27, 2016
Published: June 17, 2016

DOI: 10.1021/jacs.6b03980
J. Am. Chem. Soc. 2016, 138, 8560−8568

SECM, optimized to carry out measurements with nanometer-scale resolution, is a useful approach to study the relationship between structure and electrocatalytic activity of single nanostructures. It allows one to differentiate the average behavior of NPs in a typical ensemble measurement with that of each individual NP.[1] Nanoscale SECM requires a nanometer-sized electrode tip, with a stable nanogap between the tip and nanostructure using piezoelectric actuators for nanometer-scale lateral and vertical resolution. We report use of a nanometer-scale SECM with new methodology for the study of electrochemical activity of individual Pt NPs and their size, shape, and spatial orientations. In particular, we assess the electrocatalytic activity of the hydrogen oxidation reaction (HOR) at individual Pt NPs.[7]

In this work, we electrodeposited Pt NPs with a few tens to hundred nm radii on highly oriented pyrolitic graphite (HOPG) via nucleation and growth without aids of capping agents or anchoring molecules. Moreover, we fabricated a well-defined nanometer-sized electrode tip comparable to dimensions of NPs and achieved a stable nanogap between the tip and NPs. We carried out SECM imaging studies in these NPs with nanometer spatial resolution as well as kinetic studies to access the fast electron-transfer (ET) rates. Specifically, we used two different types of redox mediators: (1) outer-sphere mediator, a ferrocene derivative to resolve the topographical features, and (2) inner-sphere reaction, HOR to access the electrocatalytic activity of individual Pt NPs. The HOR is a very fast reaction, and the actual heterogeneous ET rate constant free of mass transfer effects has not yet been measured.[8] We devoted considerable effort in this work to addressing this important issue, finding a large effective rate constant for the HOR, k^0_{eff} of $\geq$2 cm/s. Our SECM measurements were matched with numerical simulations using a finite element method. The analytical approach described in this work can be extended to the quantitative study of other surface effects on catalytic activities of NPs, for example, in the analysis of capping agent-related effects on electrocatalytic activity.

2. EXPERIMENTAL SECTION

2.1. Chemicals and Materials. Ferrocenyl methyl trimetylammonium iodide ($FcTMA^+$ I^-), perchloric acid, and sodium perchlorate were purchased from Sigma-Aldrich and used as received. Ferrocenyl methyl trimethylammonium perchlorate ($FcTMA^+$ ClO_4^-) was prepared by metathesis. Hexachloroplatinate solution (8 wt % H_2PtCl_6 in H_2O) was purchased from Sigma-Aldrich. Hydrochloric acid, hydrogen peroxide, and sulfuric acid were obtained from Fisher Scientific and used as received. HOPG (ZYB grade, Micromasch) was used after a fresh cleavage. A Milli-Q Integral system (EDM Millipore, Berllerica, MA) was equipped to obtain ultrapure water with total organic carbon (TOC) level at <3 ppb as measured by an internally equipped TOC monitor as well as the resistivity 18.3 MΩ/cm. All the solutions for electrochemical measurement were prepared with ultrapure water and filtrated with syringe filtered with 100 nm diameter pore (Millex-Syringe driven filter unit, PVDF-0.1 μm, Merck Millipore Ltd.) except the acidic solution. All the glassware and the SECM cell made of Teflon and glass were extensively cleaned with piranha solution (1:1 ratio of H_2SO_4:H_2O_2) followed by thorough washing with ultrapure water before use.

2.2. Pt Nanoelectrode Fabrication. Pt nanoelectrodes used as nanotips in SECM were fabricated by using a CO_2-laser puller, microforge, and a focused ion beam (FIB) instrument as reported elsewhere.[9] Briefly, 25 um diameter Pt wire (Goodfellow, annealed) inserted in the borosilicate capillary (I.D. 0.2 mm, O.D. 1 mm) was pulled together with CO_2 laser puller (P-2000, Sutter). Continuously, Pt nanoelectrode was further annealed by microforge (MF-0P, Narishige, Japan) to decrease RG (a ratio between glass sheath and Pt radii) as well as a better sealing. The annealed Pt nanoelectrode was milled by FIB (FEI Strata DB235) to expose Pt disk resulting in an inlaid disk-shaped electrode with nanometer level smoothness. To avoid any damage to electrodes caused by electrostatic discharge, we handled Pt nanoelectrodes with protection tools.[10] Prepared Pt nanoelectrodes were stored in a humidity controlled box maintaining over 50% relative humidity at 22−24 °C. The Pt nanoelectrodes were also handled at over 30% relative humidity.

2.3. Electrodeposition of Pt NPs on HOPG. A CHI760E bipotentiostat (CH Instrument, Austin, TX) was used for the electrodeposition of Pt NPs with a three electrode cell configuration, where HOPG, mercury sulfate electrode (MSE), and Pt disk electrode are working, reference, and counter electrodes, respectively. First, freshly cleaved HOPG was prepared. Before immersing HOPG in the plating solution containing1 mM H_2PtCl_6, 0.1 M HCl, a constant potential at 0.27 V was held to HOPG from the air to the plating solution (or vise versa) to avoid a spontaneous deposition of Pt on HOPG.[11] Using a multiple potential step technique, a constant potential of −0.6 V vs MSE was applied to HOPG during electrodeposition for 240 s. After electrodeposition, the potential returned to the initial potential, 0.27 V, to completely stop the deposition process. For this potential control, "return to the initial potential after run" function was activated in the CHI software. To avoid damages by electrostatic discharge to either Pt NPs or HOPG, we handled HOPG with protection tools as well as using the "holding the cell on" function as reported elsewhere.[10] Also, the relative humidity was maintained over 30% at 22−24 °C. Once Pt NPs/HOPG was prepared, it was stored in ultrapure DI water in the closed cell to protect its surface from airborne contaminants before performing SECM measurements.

2.4. Instrumentation and Procedures. SECM experiments were carried out using a home-built instrument. The instrument is composed of a bipotentiostat equipped with piezoelectric actuators operated with a labview program. The positioning of the piezo and the electrochemistry are carried out independently using two different circuits as shown in the diagram in Figure 2. The bipotentiostat is in control with the CH software installed in the first computer (left computer in Figure 2). Cyclic voltammetry and chronoamperometry can be performed using this software. To move the piezos, a second computer (on the right in Figure 2) and an original Labview program are used. The piezo movement can be synchronized with the tip current by reading the analog output signal from the bipotentiostat via data acquisition board. Note that a single ground is used to avoid any ground loop issue. All of the metal parts in the isothermal room and the electronic equipment are grounded to prevent damage to the tip. To suppress a thermal drift, the entire instrument including a faraday cage and a vibration isolation table was located in an isothermal chamber.[12,13] In details, a CHI760E bipotentiostat (CH Instrument, Austin, TX) was used for electrochemical control. Particularly, all relay switches for working electrode 1 (WE1), working electrode 2 (WE2), reference electrode (RE), and counter electrode (CE) in CHI760E bipotentiostat were physically removed following manufacturer's instruction to avoid electrochemical damage of nanometer-sized Pt nanoelectrode during SECM measurements as reported elsewhere.[13] For the electrochemistry, a four electrode cell configuration was used with two Pt wires as quasireference (QRE) and counter electrodes. Highly precise x, y, and z piezoelectric actuators with a capacitive feedback loop (P-260.Z piezo, P-260.2 XY piezo, PI instruments) were mounted on the metal stage (400 series linear stage, Newport); stepping motors were replaced by the manually operated lockable micropositioner (Lockable differential micropositioner DM-25L, Newport) in the x, y, and z axes. This was done to suppress a creeping effect that is found with stepping motors, thus stabilizing the nanoelectrode position during piezo movement. The electrochemistry was operated by CHI software using the "hold the cell on" function since there are still other relays to be controlled properly, where both nanotip (Pt nanoelectrode) and substrate (HOPG) currents were recorded during the entire experiments. Simultaneously, the piezo was operated by the labview code and reading the analog current signal

DOI: 10.1021/jacs.6b03980
J. Am. Chem. Soc. 2016, 138, 8560−8568

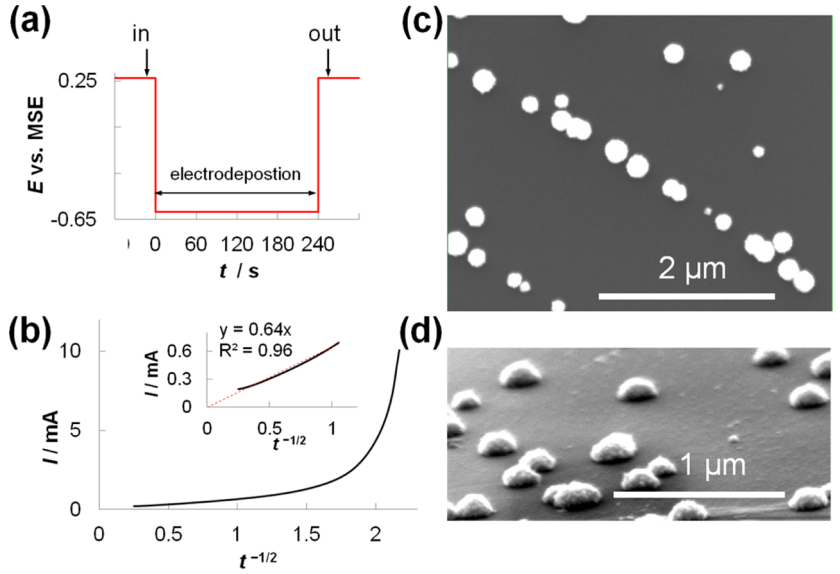

Figure 1. (a) Potential diagram employed to electrodeposition of Pt NPs on HOPG. The duration of cathodic potential pulse is 240 s. (b) The resulting current plot vs time$^{-1/2}$ during electrodeposition. The current shows a clear deviation from linearity as a function of time$^{-1/2}$ indicating a significant nonfaradaic current component (i.e., large R_uC_d) in the electrochemical cell. In the inset, linearity could be obtained in the current plot vs time$^{-1/2}$ when the time for collecting data under an electrodeposition potential becomes much greater than R_uC_d implying a simple Cottrell decay behavior under a planar diffusion control. (c,d) FE-SEM images of electrodeposited Pt NPs on HOPG in top and side view, respectively. Note that Pt NPs are preferentially deposited along the edge of HOPG.

from the CHI760E bipotentiostat through data acquisition board (USB-6009 Multifunction I/O, National Instrument), thus synchronizing the movement of piezoelectric actuators with the corresponding tip current as a function of distance between the nanotip and the substrate. For the proper connection of the nanotip under "cell on between run function", dummy voltammetry was run under RE and CE connection in the presence of electrolyte before connecting tip (WE1) or HOPG (WE2). To suppress the local thermal drift, the electrochemical cell was covered with a lid to avoid solvent evaporation during the experiment.[12] To avoid any electrode damage due to ESD, we handled the Pt nanotip and HOPG with protection tools as reported elsewhere.[10] Also, the relative humidity was maintained over 30% at 22−24 °C.

2.5. SECM Procedures and Measurement. A Pt nanoelectrode used as an SECM tip was positioned ca. 100 μm above the HOPG substrate with a lockable micropositioner in z axis under the video microscope, then micropositioners were locked. The tip was then brought closer to the substrate with the SECM approach curve technique until the feedback current appeared in the presence of either $FcTMA^+$ or H^+ in the electrolyte solution (a solution composition and potentials at the nanotip and the substrate are described below). When the z-piezoelectric actuator reached the limit of its travel distance (ca. 50 μm) before showing any feedback, the z-piezo was completely contracted, and the nanotip was manually lowered down with a micropositioner at 40 μm distance after unlocking. Then, the manipulator was locked again, and the nanotip was approached with z-piezo at 50 nm/s (5 nm/0.1 s) rate by SECM approach technique until feedback appeared. After 2−3 times of this repetitive procedure, as described above, the nanotip could be positioned ca. 20 μm above the substrate, where the z-piezoelectric actuator has enough room to expand. The fine current−distance curves were obtained at 10 nm/s (1 nm/0.1 s) rate for the subsequent fine approach. Once the nanotip approached to within a feedback, distance was comparable to the radius of the tip, then the tip current was monitored at the fixed distance. After confirming a stable tip current level at the constant height, thus forming a stable nanogap with a drift level <0.5 nm/min (see Figures 4d and S1), constant-height SECM images were obtained at 200 nm/s (20 nm/0.1 s). For the topographical study, the SECM imaging was conducted in the electrolyte solution containing 1 mM $FcTMA^+$, 10 mM $NaClO_4$, and 0.3 and −0.1 V vs Pt QRE were applied to the nanotip and Pt NP/HOPG substrate, respectively, where $FcTMA^+$ was oxidized at the nanotip and tip generated $FcTMA^{2+}$ was reduced at the substrate with diffusion controlled rates. After the SECM experiment in $FcTMA^+$, the nanotip was withdrawn in z axis with ca. 20 μm, the entire solution was flushed with ultrapure DI water thoroughly and subsequently replaced with a new electrolyte solution containing 2 mM $HClO_4$ and 10 mM $NaClO_4$ using inlet and outlet tubes installed in SECM cell. Before conducting SECM experiment for the reactivity study, preactivation was carried out to the tip and substrate by applying −0.95 V vs Pt QRE for ca. 2 h to get the well-defined voltammogram and reasonable limiting current for H^+ reduction (more details in Results section). Once a stable limiting current for H^+ reduction was obtained at the nanotip, the tip was continuously approached with z-piezo within the feedback distance and scanned laterally to get the constant-height SECM image based on H^+ reduction/H_2 oxidation over the same location as studied with the $FcTMA^{2+}$/$FcTMA^+$ couple. For this SECM image, − 1.0 and −0.4 V vs Pt QRE were applied to the tip and Pt NP/HOPG, respectively, where H^+ was reduced at the nanotip and tip generated H_2 was oxidized at the Pt NPs on HOPG substrate. Specifically, − 0.4 V vs Pt QRE for HOPG substrate is the potential before forming Pt oxide (see Figure S6). All experiments were carried out in the isothermal chamber at a relative humidity maintained over 40% at 22 °C.

3. RESULTS

3.1. Characteristics of Pt NPs Electrodeposited on HOPG. We electrodeposited Pt NPs on the HOPG surface to study the electrocatalytic activity in HOR at the single NP level. HOPG offers a smooth and flat surface with a uniform conductivity across its surface. Additionally, HOPG is inert for various catalytic reactions, thus providing an excellent substrate for studying the catalytic activity of nanomaterials without a significant interference in the SECM setup. The subnanometer-scale roughness of bare HOPG was reported previously with an SECM imaging technique as well as an AFM study.[14] In this work, we electrodeposited Pt NPs on HOPG as reported elsewhere.[11] As shown in Figure 1a, because of reducing sights Pt particles can deposit spontaneously on HOPG; this

DOI: 10.1021/jacs.6b03980
J. Am. Chem. Soc. 2016, 138, 8560−8568

spontaneous deposition was avoided by holding the potential at 0.27 V vs MSE. The HOPG was moved from the air to the plating solution before electrodeposition or moved from the plating solution to the air after electrodeposition. For the electrodeposition, a constant long plating pulse was applied to the HOPG as −0.6 V for 240 s. The resulting current shows a clear deviation from linearity as a function of time$^{-1/2}$ indicating a significant nonfaradaic current component in the electrochemical cell, probably originating from a large product of uncompensated resistance (R_u) and double layer capacitance (C_d), i.e., a cell characteristic time constant (Figure 1b). When the time for collecting data under an electrodeposition potential becomes much greater than R_uC_d, linearity could be obtained in the current plot vs time$^{-1/2}$, implying a simple Cottrell decay behavior under a planar diffusion control (the inset in Figure 1b).[15]

After the deposition of Pt under a constant potential, Pt NPs were directly observed by the field emission-scanning electron microscopy (FE-SEM) as it could be employed to image a large area over HOPG. Well-defined hemisphere to sphere-shaped Pt NPs with 90 ± 30 nm radii were observed in Figure 1c. Interestingly, a uniform height of ca. 120 nm could be seen while various aspect ratios were measured, indicating that Pt NPs are spread out once they reached the steady-state height during nucleation and growth (Figure 1d). The deposited Pt NPs have a distinct feature of a highly preferential deposition on the edges of HOPG as reported by Penner and coworkers.[11] A lower density of Pt NPs on a basal plane of HOPG was observed, while an array of Pt NPs at a step edge of HOPG could be seen in Figure 1c.

Figure 1c shows that the Pt NPs are at a fairly low density with well-resolved NPs without aggregation, which is required for SECM measurements of the electrocatalytic activity at individual NPs. In addition, the direct nucleation and growth of Pt NPs leads to an intrinsically robust immobilization on the HOPG surface, hence no additional anchoring molecules were needed. In that sense, the electrodeposition technique allows for a simple preparation of Pt NPs with less complexity, that is, well-resolved Pt NPs with well-defined geometry strongly immobilized on HOPG without aid of capping agents or anchoring molecules.

3.2. SECM Imaging of Topography and Electrocatalytic Activity. We employed SECM with an inlaid disk Pt nanotip to image individual Pt NPs by mapping electrochemical reactions at their surface. In Figure 2, a schematic diagram of our nanoscale SECM is displayed (detailed information is in Experimental Section and SI and is reported elsewhere[13]). SECM is a powerful technique to study the local reactivity. It, however, convolutes the topographic information with electrochemical activity. To resolve the topographic information and electrochemical activity of Pt NPs and study them independently, we performed two consecutive SECM experiments using two different redox mediators: (1) $FcTMA^+$ undergoing outer-sphere ET reaction under masstransfer limiting conditions and (2) H^+ undergoing inner-sphere ET reaction. As schematically shown in Figure 3, each different ET reaction is studied at the same Pt NPs using Pt nanotip comparable to the radius of Pt NPs. First, we carried out measurements using $FcTMA^+$. When the distance between the Pt nanotip and substrate surface also becomes comparable to the radius of Pt nanotip, the $FcTMA^{2+}$ generated at Pt nanotip can be reduced back to the original form of $FcTMA^+$ at both HOPG and Pt NPs at a rate governed by diffusion, because the

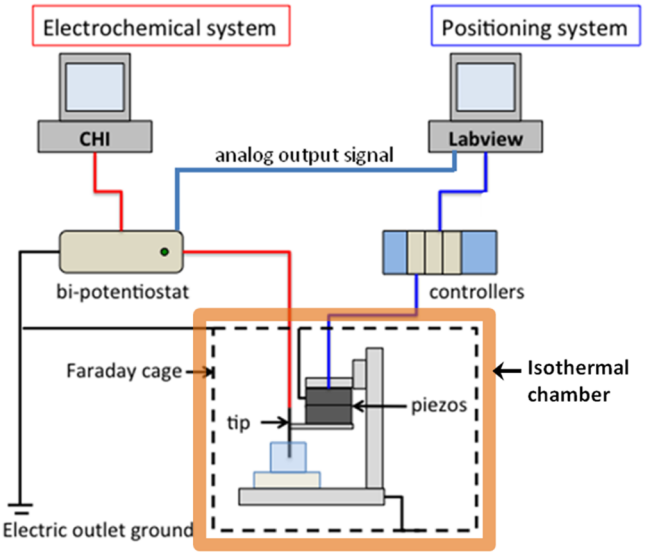

Figure 2. A schematic diagram of nanoSECM.

heterogeneous ET reaction of this mediator is not sensitive to the catalytic activity of the different surfaces. Consequently, the tip current during the SECM imaging at constant height is only determined by the distance separation between the tip and the target (NP or HOPG substrate), thus providing topographic information. Second, we carried out measurements using HOR, an inner-sphere ET reaction that is more selective to the surface catalytic property.[16] With this reaction, H_2 molecules generated at the Pt nanotip cannot be oxidized back to H^+ at HOPG, but they are selectively oxidized at the Pt NP surface. Accordingly, the tip current over Pt NPs during SECM imaging contains information on the catalytic activity on HOR as well as topography, thereby a catalytic activity of Pt NP can be solely extracted after resolving the topographic information determined from the first study with $FcTMA^+$.

Based on the above strategy, the freshly prepared Pt NPs electrodeposited on HOPG were studied by SECM with $FcTMA^+$, first. The voltammograms of Pt nanotip and Pt NPs/HOPG substrate in 1 mM $FcTMA^+$, 10 mM $NaClO_4$ are shown in Figure 4. The radii of FIB milled Pt nanotip and glass sheath were determined by scanning electron microscopy (SEM) which agreed with the current in the bulk solution, i_{ss} as given by

$$i_{ss} = 4xnFDCa$$

where x is a function of RG (ratio between glass sheath and Pt disk radius), n (=1) is the number of transferred electrons in the tip reaction, F is the Faraday constant, D is diffusion coefficient of redox mediator ($D_{FcTMA^+} = 6 \times 10^{-6}$ cm^2/s),[17] C is the concentration of redox mediator, (C = 1 mM), and a is the radius of Pt nanotip. The resulting radius of Pt nanotip was 90 nm, showing i_{ss} = 22 pA. A peak separation of ∼80 mV is obtained in the voltammogram of Pt NPs/HOPG substrate, slightly deviating from the reversible one ET reaction (60 mV) attributed to the IR drop originating from the low concentration of supporting electrolytes.

A current vs distance curve was recorded using E_{tip}= 0.3 V and $E_{substrate}$ = −0.1 V vs Pt QRE (Figure 4d). Theoretical fitting of the data indicated that the tip was placed at 210 nm above the HOPG substrate (with positive feedback current of 26.3 pA). As shown in the inset of Figure 4d, a stable tip

DOI: 10.1021/jacs.6b03980
J. Am. Chem. Soc. 2016, 138, 8560−8568

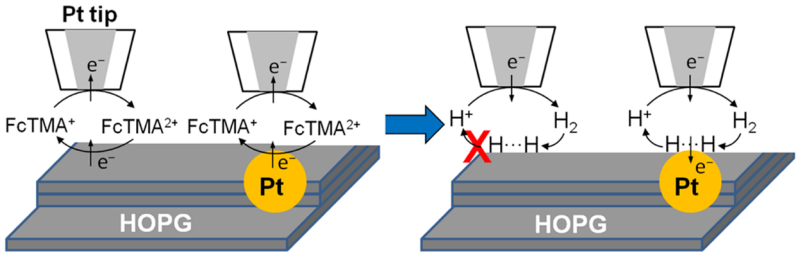

Figure 3. Schemes illustrating ET reactions occurring at Pt NP and HOPG in the presence of $FcTMA^+$ (left) or H^+ (right).

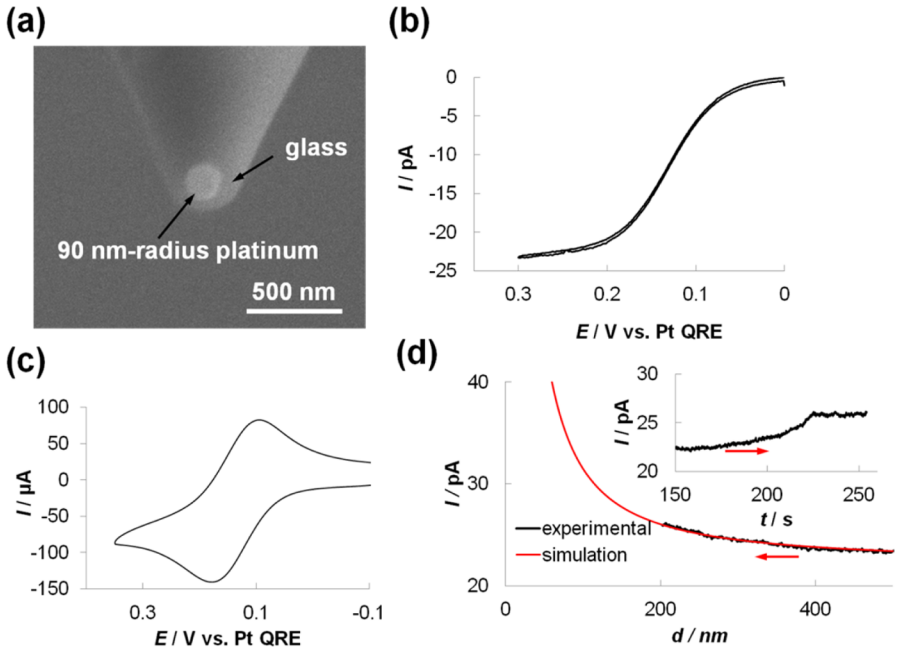

Figure 4. (a) SEM image of FIB milled Pt nanotip. (b, c) Voltammograms of Pt nanotip and PtNPs/HOPG substrate in 1 mM $FcTMA^+$ and 10 mM $NaClO_4$ with Pt QRE and Pt CE, respectively. (d) SECM approach curves of Pt nanotip over HOPG obtained at the rate, 10 nm/s, where E_{tip} and $E_{substrate}$ are held at 0.3 V and −0.1 V vs Pt QRE, respectively. Experimental curve was fitted with theoretical positive feedback curve. In the inset, the current transient with time is shown, where tip approached to 210 nm above HOPG and stop approaching. At this fixed distance, the tip current was monitored to ensure a stable nanogap before SECM imaging. The arrows denote the approaching direction of a Pt nanotip over HOPG.

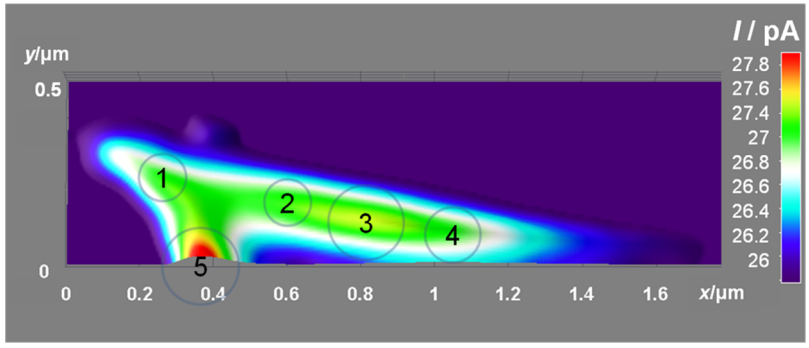

Figure 5. SECM image of $FcTMA^+/FcTMA^{2+}$ ET reaction at Pt NPs in 1 mM $FcTMA^+$, 10 mM $NaClO_4$ with E_{tip} = 0.3 V, $E_{substrate}$ = −0.1 V vs Pt QRE. Pt nanotip was scanned at 200 nm/s. Five Pt NPs are denoted in the overlapped image.

current was monitored to ensure the stable nanogap after approaching the Pt nanotip at 210 nm position before SECM imaging. Subsequently, a constant-height SECM image with dimensions 3 × 0.5 μm was taken using a scanning rate of 200 nm/s (Figure 5). This image showed enhanced currents from the feedback above Pt NPs up to 28.1 pA. Thus, four Pt NPs along a step edge of HOPG show a rather uniform increase in current rather than resolved Pt NPs. Also, the far tip distance from Pt NPs could overlap the SECM image significantly due to broadening of the diffusion layer over Pt NPs. We predicted five NPs from the prominent peak currents in the convoluted SECM images as denoted in Figure 5.

After the first series of measurement with the $FcTMA^+/FcTMA^{2+}$ couple, the Pt nanotip was retracted up to 20 μm in the z direction. Subsequently, the electrolyte solution in the SECM cell, which contained two inlet and outlet tubes, was

DOI: 10.1021/jacs.6b03980
J. Am. Chem. Soc. 2016, 138, 8560−8568

carefully flushed with deionized water which was then completelly replaced with a new electrolyte solution containing 2 mM $HClO_4$ and 10 mM $NaClO_4$, thus maintaining the position of Pt nanotip after the first SECM measurement. After completing the electrolyte replacement, a Pt activation process was performed on a Pt nanotip by applying −0.95 V vs Pt QRE for ca. 2 h to get the well-defined voltammogram and reasonable limiting current for H^+ reduction (Figure 6). The

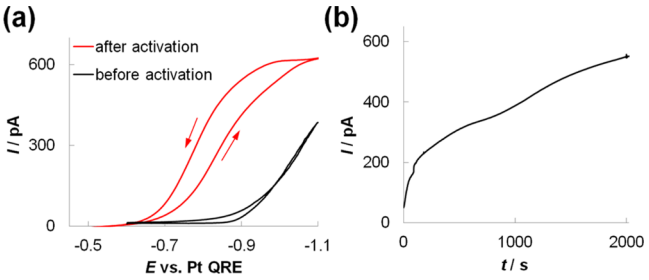

Figure 6. (a) Voltammograms of Pt nanotip in 2 mM $HClO_4$ and 10 mM $NaClO_4$ before (black curve) and after preactivation (red curve). (b) Chronoamperometric curve for preactivation of Pt nanotip, where E_{tip} = −0.95 V vs Pt QRE applied for ca. 2 h in 2 mM $HClO_4$ and 10 mM $NaClO_4$.

resulting voltammograms for a Pt nanotip before and after preactivation step are shown in Figure 6a. After the activation step, a reasonable tip current (i_{ss} = 600 pA, D_{H^+} = 8 × 10^{-5} cm^2/s, see ref 18) at a given size of a Pt nanotip was observed in the voltammogram with significant hysteresis; no discernible fouling of a Pt nanotip was observed over time. Without a proper activation step, the tip current for H^+ reduction was unstable and gradually decreased (data not shown). Such an activation step at cathodic potential could generate reactive oxygen species such as hydroxyl radicals ($OH^•$) as a result of oxygen reduction, thus decomposing organic contaminants on the Pt surface[19,20] and cleaning its surface to be active for H^+ reduction/H oxidation reaction. We also treated Pt NPs on HOPG in the same way as the Pt nanotip before SECM experiments. The quantitatively reasonable tip current for H^+ reduction suggested that deaeration was unnecessary; the resulting H^+ reduction current was about 27 times higher than the current expected from oxygen reduction in air-saturated solution.

Once the tip current became stable at a constant potential of −1.0 V vs Pt QRE, a current−distance curve was recorded using −1.0 and −0.4 V vs Pt QRE at E_{tip} and $E_{substrate}$, respectively. Instead of the expected diffusion controlled pure negative feedback behavior, over noncatalytic HOPG, the resulting current−distance curve showed a shape with only a small feedback change from the limiting current in the bulk solution (see Figure S3c). We attribute this behavior to the presence of small Pt "nuclei" electrodeposited on the HOPG. In SEM observation, the presence of such Pt nuclei on the HOPG was consistent with a change in contrast of the HOPG surface after the electrodeposition. Using the finite element analysis, we simulated the theoretical current−distance curve where the Pt UME nanotip approached over the Pt nuclei with ca. 3 nm height as active spots sitting on the inert substrate (detailed information in SI). Based on theoretical curves, we estimated the coverage of Pt spots under the Pt nanotip as ca. 1%.

We could also measure an accurate tip distance from the HOPG thus approaching the Pt nanotip to 134 nm over HOPG. The Pt nanotip was laterally scanned continuously over the same area previously studied with $FcTMA^+$. The resulting 1.8 × 0.5 μm^2 constant-height SECM image obtained at 200 nm/s scan rate shows enhanced feedback currents over Pt NPs up to 2 nA as a result of HOR at Pt NP surface (Figure 7). In this image, the Pt NPs are resolved better than those obtained to the SECM image taken with $FcTMA^+$ because of the closer tip distance, thus less broadening of the diffusion layer over each Pt NP. Importantly, we observed the same set of Pt NPs in this SECM image observed in the first SECM image with $FcTMA^+$. However, there was a slight drift in lateral direction between the two SECM image measurements, thereby the scanned area was slightly offset from the previously studied area. As a result, the fifth Pt NP was largely off the measured SECM image. We denoted the numbers of Pt NPs corresponding to the ones studied with $FcTMA^+$. Notably, the shape of the Pt NPs in the SECM image appears to have an ellipsoidal shape. We discuss more details about the shape of Pt NPs in the Discussion section and SI.

4. DISCUSSION

4.1. Topographic Features: Size and Spatial Orientation of NPs. We analyzed the SECM image taken with $FcTMA^+$ quantitatively to extract topographical information on the Pt NPs such as the dimension and spatial orientations. The electrodeposited Pt NPs had a unique feature in SEM images of having a uniform height as ca. 120 nm but a different aspect ratio between the height and radius among the different Pt NPs (Figure 1c,d). Accordingly, we fixed the height of NP as 120 nm. Subsequently, the only remaining factor to determine the tip current over the Pt NPs is the radius of NPs. Mirkin and co-

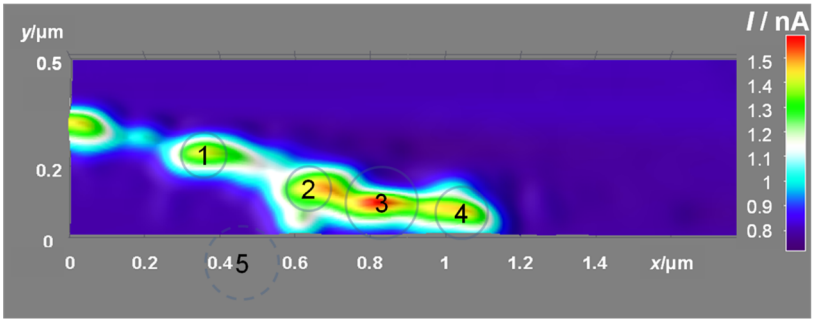

Figure 7. SECM image of H^+/H ET reaction at Pt NPs in 2 mM $HClO_4$ and 10 mM $NaClO_4$ with E_{tip} = −1.0 V, $E_{substrate}$ = −0.4 V vs Pt QRE. Pt nanotip was scanned at 200 nm/s. Five Pt NPs are denoted in the SECM image.

DOI: 10.1021/jacs.6b03980
J. Am. Chem. Soc. 2016, 138, 8560−8568

workers have reported a theoretical analysis for the size effect of an individual NP on the tip current in SECM measurement.[21] Using the same theoretical approach, we could predict the current−distance curves over the Pt NPs by varying the radii of Pt NPs, where the resulting tip current over NP is governed by diffusion control as shown in Figure 8. Since the distance

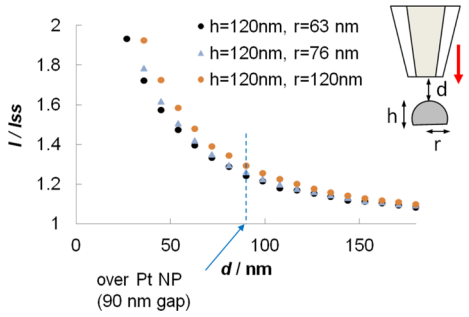

Figure 8. Theoretical current−distance curves for an inlaid-disk tip with RG 2.5 approaching a reactive hemispherical to spherical NP with dimensions, h (= height) and r (= radius), on the inert HOPG substrate, and d represents the gap between the tip and apex of spherical NP. The resulting tip current over NP is governed by diffusion control in this analysis.

between tip and HOPG substrate was 210 nm in the constant-height SECM image taken with $FcTMA^+$, the separation gap, d, between the tip and 120 nm high Pt NP was 90 nm. By comparing the currents measured in our images vs the currents obtained in numerical simulations at gaps of 90 nm (Figure 8), we determined the radii of the five Pt NPs seen in Figure 5 to be 63, 63, 108, 76, 117 nm, in order from first to fifth as noted in the figure. Notably, ±10 nm deviation in the NP height causes only ±0.4% deviation in simulated tip currents at any gap between the tip and NP, so it is insignificant in influencing the tip current in our topographical analysis.

Using the NP dimensions previously determined, we performed numerical simulations in 3D space to define the spatial location of the NPs with respect to each other and to predict the current vs lateral distance profiles that the array of NPs seen in Figure 5 would generate along the x axis at a given 90 nm gap between the tip and NPs. The theoretical currents along the x axis at three different locations (i.e., at a, b, and c) were simulated and compared with the experimental current profiles from the cross-sectional current response in the SECM image as presented in Figure 9. Agreement between the theoretical and experimental current profiles was obtained, validating our determination of NP sizes and the spatial orientation.

4.2. Electrocatalytic Activity of Pt NPs for HOR. We also analyzed the SECM image studied with H^+ quantitatively to estimate the electrocatalytic activity of each Pt NP in HOR. The SECM image with H^+ was obtained at a constant height of 134 nm from the HOPG, giving a separation gap of 14 nm between a Pt nanotip and Pt NPs. At a given 14 nm gap, a theoretical tip current can be predicted over Pt NP with determined dimensions, where the ET reaction at Pt NPs is governed by diffusion control in this analysis. Subsequently, the experimental and theoretical current profiles in the y axis were compared to study the isolated Pt NPs. As presented in Figure 10, agreement in current magnitude over three different Pt NPs could be observed, implying that H_2 generated at the Pt

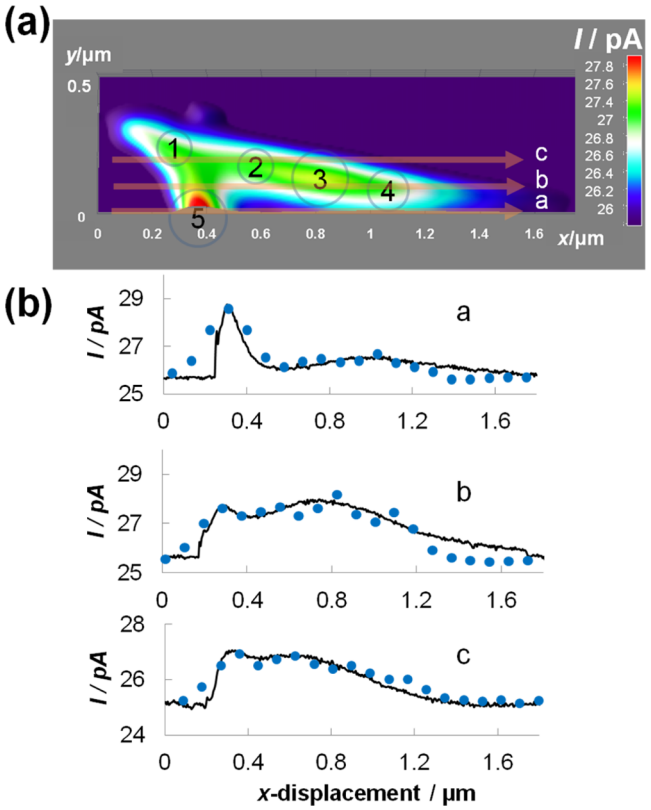

Figure 9. (a) SECM image for $FcTMA^{2+}/FcTMA^+$ couple and denoted three different lateral location of a, b and c for cross-sectioning. (b) Cross-sectional current responses at each different location from SECM image in a panel. The experimental curves (solid lines) show a good fit with theoretical simulation (closed circles), where the ET reaction at Pt NPs is governed by the diffusion control in this analysis.

nanotip is instantaneously oxidized at the Pt NPs as soon as it diffuses to their surface.

When the gap (d) between the tip and the substrate is smaller than the tip radius (a) in the SECM configuration, the mass transfer rate (m) is determined by the gap instead of the tip radius, thus $m = D/d$ (D = diffusion coefficient of the reactant). With a 14 nm gap between Pt nanotip and Pt NPs during constant-height SECM imaging, the resulting mass transfer rate could be enhanced up to 26 cm/s with a given diffusion coefficient ($D_{H_2} = 3.7 \times 10^{-5}$ cm^2/s).[7] Generally, a mass transfer controlled condition is obtained when the corresponding heterogeneous ET rate is at least an order of magnitude larger than the mass transfer rate.[15] Assuming a Butler−Volmer relationship, we could extract a lower limit of the heterogeneous effective rate constant for HOR, $k^0_{eff} \geq 2$ cm/s with $\alpha = 0.5$ and potential differentce ($E - E^{0\prime}$) = ca. 250 mV. This lower limit rate constant was validated by fitting the voltammograms obtained at a Pt nanotip (see Figure S5).

Previously a heterogeneous rate constant of at least 0.22−0.42 cm/s for the HOR was reported by employing steady-state SECM measurements, where the ET step (Volmer reaction) was considered as a rate-limiting step based on the obtained Tafel slope of ca. 118 mV.[16,22] In fact, the HOR on Pt has been broadly accepted as one of the fastest ET reactions. So far, ca. k^0_{eff} of ≥0.9 cm/s has been reported by Kucernak and co-workers using a floating electrode with a Pt NP ensemble under highly enhanced mass transfer condition.[23] Notably, the large

DOI: 10.1021/jacs.6b03980
J. Am. Chem. Soc. 2016, 138, 8560−8568

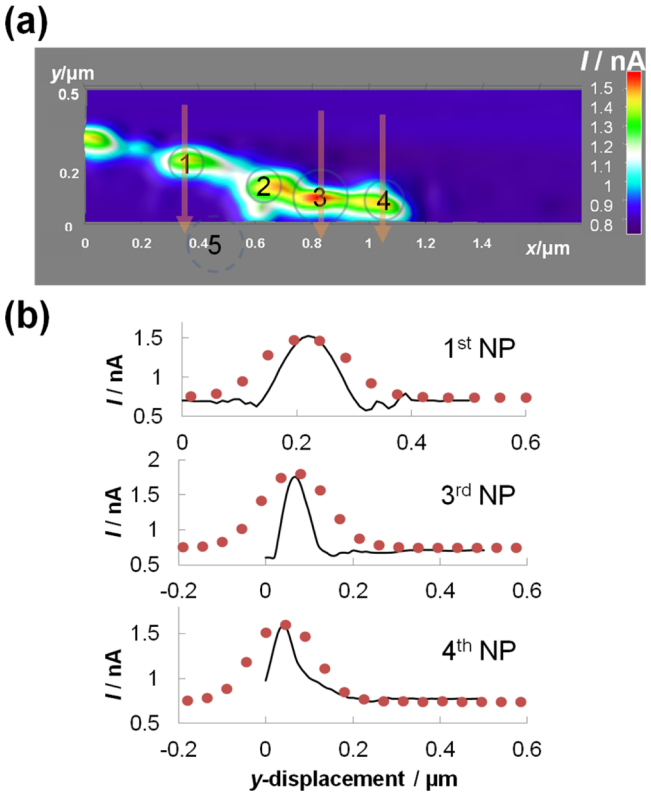

Figure 10. (a) SECM image for H^+/H_2 couple and denoted three different locations such as first, third, and fourth Pt NPs for cross-sectioning in y axis. (b) Cross-sectional current responses at each different location from SECM image in a panel. The experimental curves (solid lines) fit well with theoretical simulation (circles) in terms of current magnitudes, where the ET reaction at Pt NPs is governed by diffusion control in this analysis. A discrepancy, however, is seen in current peak width.

k^0_{eff} in our work was obtained at each individual Pt NP, not an ensemble. We did not observe a discernible variation in the reactivity between different sizes of Pt NPs from 63 to 120 nm radii; significant variation in oxygen reduction activity depending on the size has been reported in electrodeposited Pt NPs in scanning electrochemical cell microscopy (SECCM) study.[24] However, such variation might also be attributed to airborne contaminants on the surface of Pt NPs in SECCM originating from the inherent experimental setup. Indeed, Amemiya and co-workers recently reported the importance of organic contamination and cleaness of electrode surface in their ET kinetic study.[17] In this regard, we also tried to keep the surface of the tip and the Pt NPs/HOPG clean in the present nanoscale SECM by using ultrapure water with TOC level <3 ppb, minimum exposure of their surfaces to the air with storing in ultrapure water, and the preactivation process. Such experimental conditions enabled us to measure reproducible electrocatalytic activity of Pt NPs in HOR over the size difference by a factor of 2. In a study of the effect of Pt NP size on its catalytic activity, a size over a large range, at least an order of magnitude, may be needed. Moreover, there may be a critical size region where such a size effect on the catalytic activity is exhibited.[25] Thus, nanoSECM provides a versatile approach to varying the dimension of Pt NPs and the Pt nanotip flexibly up to the tens of nanometer regime.

Note that there is a discrepancy in the current peak width between theoretical and experimental current profiles over Pt NPs for HOR study, whereas a good agreement in current magnitudes is obtained under diffusion controlled conditions. Accordingly, Pt NPs in SECM images appear to have elongated shapes. As shown in SI, the apparent ellipsoidal shape of the NPs is caused by an artifact due to a tip drift in the lateral direction during tip scanning. Such an artifact could be successfully suppressed by replacing general positioners without locks with lockable positioners in x and y axes, thereby a spherical shape of an individual NP could be attained in SECM image studied with $FcTMA^+$ as presented in Figure 11 (detailed information in SI).

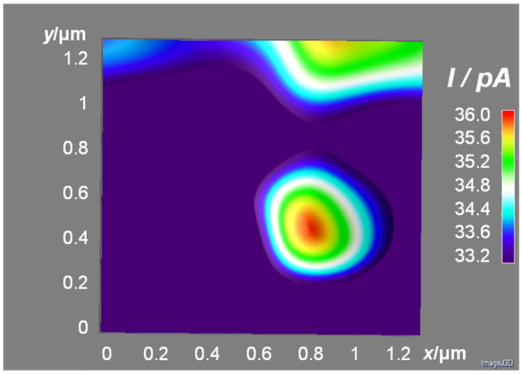

Figure 11. SECM image of an individual Pt NP obtained in 1 mM $FcTMA^+$ and 10 mM $NaClO_4$ with E_{tip} = 0.3 V, $E_{substrate}$ = −0.1 V vs Pt QRE. Pt nanotip was scanned at 200 nm/s.

5. CONCLUSIONS

We present an approach based on SECM for the study of geometric parameters and electrocatalytic activity of individual Pt NPs, with nanometer spatial resolution. For this, we electrodeposited Pt NPs of 60−120 nm radii on HOPG via a nucleation and growth path without using of capping agents or anchoring molecules. A large effective rate constant of HOR, k^0_{eff} of ≥2 cm/s could be determined owing to the enhanced mass transfer rate by forming the reliably attainable nanometer-sized gap between the nanometer-sized SECM tip and the catalytic Pt NPs. We described how to separate topographic information from catalytic activity by using two different types of redox mediators: (1) outer-sphere mediator and (2) inner-sphere mediators, thereby the SECM imaging technique was successfully employed to investigate the size, shape, spatial orientation, and the electrocatalytic activity of Pt NPs at an individual level. The analytical approach presented in this work can be used in general for the study of size and structural effects on the catalytic activity for a variety of metal NPs. Moreover, this approach can be extended to the quantitative study of surface property effects on the catalytic reactivity of NPs such as capping agent effects for an optimum catalytic property.

■ ASSOCIATED CONTENT

Supporting Information

The Supporting Information is available free of charge on the ACS Publications website at DOI: 10.1021/jacs.6b03980.

Experimental details and data (PDF)

■ AUTHOR INFORMATION

Corresponding Author

*ajbard@mail.utexas.edu

DOI: 10.1021/jacs.6b03980
J. Am. Chem. Soc. 2016, 138, 8560−8568

Notes

The authors declare no competing financial interest.

■ ACKNOWLEDGMENTS

We acknowledge support of this research from the AFOSR MURI (FA9550-14-1-0003) and the Robert A. Welch Foundation (F-0021). Also, authors thank Tim Hooper (thooper@cm.utexas.edu) for the helpful discussion in instrument design and modification (the Department of Chemistry and Biochemistry, The University of Texas at Austin). We also thank Damon Smith (damonsmith@mail.utexas.edu) for the support related to a dual beam FIB instrument (the Department of Chemical Engineering, Texas Materials Institute, Center for Nano & Molecular Science and Technology) and NSF, the petroleum Research Fund, and Welch Foundation in support of the facilities utilized in this work.

■ REFERENCES

(1) Bard, A. J.; Mirkin, M. V. *Scanning Electrochemical Microscopy*, 2nd ed.; CRC: Boca Raron, FL, 2012.
(2) Shen, M.; Ishimatsu, R.; Kim, J.; Amemiya, S. *J. Am. Chem. Soc.* **2012**, *134*, 9856−9859.
(3) Murray, R. W. *Chem. Rev.* **2008**, *108*, 2688−2720.
(4) Shao, Y.; Cheng, Y.; Duan, W.; Wang, W.; Lin, Y.; Wang, Y.; Liu, J. *ACS Catal.* **2015**, *5*, 7288−7298.
(5) Somorjai, G. A.; Park, J. Y. *Angew. Chem., Int. Ed.* **2008**, *47*, 9212−9228.
(6) Li, Y.; Somorjai, G. A. *Nano Lett.* **2010**, *10*, 2289−2295.
(7) Chen, S.; Kucernak, A. *J. Phys. Chem. B* **2004**, *108*, 13984−13994.
(8) Neyerlin, K. C.; Gu, W. B.; Jorne, J.; Gasteiger, H. A. *J. Electrochem. Soc.* **2007**, *154*, B631.
(9) Kim, J.; Izadyar, A.; Nioradze, N.; Amemiya, S. *J. Am. Chem. Soc.* **2013**, *135*, 2321−2329.
(10) Nioradze, N.; Chen, R.; Kim, J.; Shen, M.; Santhosh, P.; Amemiya, S. *Anal. Chem.* **2013**, *85*, 6198−6202.
(11) Zoval, J. V.; Lee, J.; Gorer, S.; Penner, R. M. *J. Phys. Chem. B* **1998**, *102*, 1166−1175.
(12) Kim, J.; Shen, M.; Nioradze, N.; Amemiya, S. *Anal. Chem.* **2012**, *84*, 3489−3492.
(13) Kim, J.; Renault, C.; Arroyo-Currás, N.; Nioradze, N.; Leonard, K. C.; Bard, A. J. *Anal. Chem.*, submitted.
(14) Sun, T.; Yu, Y.; Zacher, B. J.; Mirkin, M. V. *Angew. Chem., Int. Ed.* **2014**, *53*, 14120−14123.
(15) Bard, A. J.; Faulkner, L. R. *Electrochemical Methods: Fundamentals and Applications*, 2nd ed.; John Wiley & Sons: New York, 2001.
(16) Zhou, J.; Zu, Y.; Bard, A. J. *J. Electroanal. Chem.* **2000**, *491*, 22−29.
(17) Nioradze, N.; Chen, R.; Kurapati, N.; Khcataeva-Domanov, A.; Mabic, S.; Amemiya, S. *Anal. Chem.* **2015**, *87*, 4836−4843.
(18) Zhang, C.; Knyazev, D. G.; Vereshaga, Y. A.; Ippoliti, E.; Nguyen, T. H.; Carloni, P.; Pohl, P. *Proc. Natl. Acad. Sci. U. S. A.* **2012**, *109*, 9744−9749.
(19) Noël, J.-M.; Latus, A.; Lagrost, C.; Volanschi, E.; Hapiot, P. *J. Am. Chem. Soc.* **2012**, *134*, 2835−2841.
(20) Yue, Q.; Zhang, K.; Chen, X.; Wang, L.; Zhao, J.; Liu, J.; Jia, J. *Chem. Commun.* **2010**, *46*, 3369−3371.
(21) Yu, Y.; Sun, T.; Mirkin, M. V. *Anal. Chem.* **2015**, *87*, 7446−7453.
(22) Zoski, C. G. *J. Phys. Chem. B* **2003**, *107*, 6401−6405.
(23) Zalitis, C. M.; Sharman, J.; Wright, E.; Kucernak, A. R. *Electrochim. Acta* **2015**, *176*, 763−776.
(24) Lai, S. C. S.; Dudi, P. V.; Macpherson, J. V.; Unwin, P. R. *J. Am. Chem. Soc.* **2011**, *133*, 10744−10747.
(25) Auffan, M.; Rose, J.; Bottero, J.-Y.; Lowry, G. V.; Jolivet, J.-P.; Wiesner, M. R. *Nat. Nanotechnol.* **2009**, *4*, 634−641.

DOI: 10.1021/jacs.6b03980
J. Am. Chem. Soc. 2016, 138, 8560−8568